Understanding climate change projections for precipitation over western Europe with a weather typing approach

AGU PUBLICATIONS

JGR

Journal of Geophysical Research: Atmospheres

RESEARCH ARTICLE
10.1002/2015JD024399

Key Points:
- Eight weather types (WTs) largely control precipitation over western Europe
- Changes in WT frequencies and rainfall intensity explain precipitation trends
- A WT-independent background signal is identified in precipitation projections

Supporting Information:
- Figures S1–S4 and Tables S1–S4

Correspondence to:
J. A. Santos,
jsantos@utad.pt

Citation:
Santos, J. A., M. Belo-Pereira, H. Fraga, and J. G. Pinto (2016), Understanding climate change projections for precipitation over western Europe with a weather typing approach, *J. Geophys. Res. Atmos.*, *121*, 1170–1189, 1170–1189, doi:10.1002/2015JD024399.

Received 24 OCT 2015
Accepted 7 JAN 2016
Accepted article online 11 JAN 2016
Published online 8 FEB 2016

Understanding climate change projections for precipitation over western Europe with a weather typing approach

João A. Santos[1], Margarida Belo-Pereira[2], Helder Fraga[1], and Joaquim G. Pinto[3,4]

[1]Centre for the Research and Technology of Agro-Environmental and Biological Sciences, CITAB, Universidade de Trás-os-Montes e Alto Douro, UTAD, Vila Real, Portugal, [2]Instituto Português do Mar e da Atmosfera, Lisboa, Portugal, [3]Department of Meteorology, University of Reading, Reading, UK, [4]Institute for Geophysics and Meteorology, University of Cologne, Cologne, Germany

Abstract Precipitation over western Europe (WE) is projected to increase (decrease) roughly northward (equatorward) of 50°N during the 21st century. These changes are generally attributed to alterations in the regional large-scale circulation, e.g., jet stream, cyclone activity, and blocking frequencies. A novel weather typing within the sector (30°W–10°E, 25–70°N) is used for a more comprehensive dynamical interpretation of precipitation changes. A *k*-means clustering on daily mean sea level pressure was undertaken for ERA-Interim reanalysis (1979–2014). Eight weather types are identified: S1, S2, S3 (summertime types), W1, W2, W3 (wintertime types), B1, and B2 (blocking-like types). Their distinctive dynamical characteristics allow identifying the main large-scale precipitation-driving mechanisms. Simulations with 22 Coupled Model Intercomparison Project 5 models for recent climate conditions show biases in reproducing the observed seasonality of weather types. In particular, an overestimation of weather type frequencies associated with zonal airflow is identified. Considering projections following the (Representative Concentration Pathways) RCP8.5 scenario over 2071–2100, the frequencies of the three driest types (S1, B2, and W3) are projected to increase (mainly S1, +4%) in detriment of the rainiest types, particularly W1 (−3%). These changes explain most of the precipitation projections over WE. However, a weather type-independent background signal is identified (increase/decrease in precipitation over northern/southern WE), suggesting modifications in precipitation-generating processes and/or model inability to accurately simulate these processes. Despite these caveats in the precipitation scenarios for WE, which must be duly taken into account, our approach permits a better understanding of the projected trends for precipitation over WE.

1. Introduction

Spatial-temporal variability of precipitation and its extremes over western Europe (henceforth WE) is largely driven by the large-scale atmospheric flow over the Euro-Atlantic sector. This is documented by the significant relationships between precipitation and teleconnection patterns [*Barnston and Livezey*, 1987; *Hurrell and VanLoon*, 1997; *Casanueva et al.,* 2014], namely, the North Atlantic Oscillation (NAO) and East Atlantic (EA) patterns or the significant modes of coupled variability between mean sea level pressure (MSLP) and daily precipitation [*Ulbrich et al.,* 1999; *Qian et al.,* 2000; *Santos et al.,* 2007b]. From a synoptic viewpoint, large-scale anomalies associated with cyclones and blocking systems are particularly relevant for precipitation extremes in WE [*Pfahl and Wernli*, 2012; *Pfahl*, 2014; *Ramos et al.,* 2014b]. The occurrence of clusters of extratropical cyclones over the eastern North Atlantic leads to particularly stormy conditions over WE [*Pinto et al.,* 2014] and may lead to very rainy periods and floods like in the winter of 2013/2014 in the UK [*Huntingford et al.,* 2014]. Precipitation is often associated with tropical moisture exports to the extratropics [*Knippertz and Wernli*, 2010], often organized in filaments of high water vapor content (denominated "atmospheric rivers") emerging beneath the warm conveyor belts of extratropical cyclones [*Dacre et al.,* 2014]. Their role on precipitation over WE was highlighted, but their relative importance has also been questioned [*Champion et al.,* 2015; *Ramos et al.,* 2015].

The variability of the midlatitude eddy-driven jet over the North Atlantic, reflected by its mean latitude and strength, is a key forcing mechanism of synoptic variability in the Euro-Atlantic atmospheric circulation [e.g., *Woollings et al.,* 2011; *Santos et al.,* 2013], including the NAO and EA [*Woollings et al.,* 2010]. While extreme opposite behavior in the North Atlantic eddy-driven jet often triggers precipitation extremes over

WE [e.g., *Andrade et al.,* 2011; *Harnik et al.,* 2014], there is no clear climate change footprint in the jet variability during the twentieth century over the North Atlantic and Europe [*Barnes and Polvani*, 2013; *Woollings et al.,* 2014]. The complexity of the dynamical mechanisms underlying the jet stream and storm track variability can be highlighted by the number of different interactions over a wide range of different temporal and spatial scales, such as large-scale eddies [*Santos et al.,* 2009a], Rossby wave breaking [*Woollings et al.,* 2011; *Masato et al.,* 2012; *Barnes and Polvani*, 2013], atmospheric blocking [*Davini et al.,* 2014b], troposphere-stratosphere couplings [*Santos et al.,* 2009b; *Davini et al.,* 2014a; *Kidston et al.,* 2015], Arctic ice and snow coverage [*Screen*, 2013; *Cohen et al.,* 2014], latent heat release [*Wernli et al.,* 2002; *Ludwig et al.,* 2014], or ocean fronts [*Small et al.,* 2014]. Therefore, climate models need to properly integrate most of these interactions to realistically simulate the large-scale circulation in the Euro-Atlantic sector. For instance, climate models unable to accurately reproduce troposphere-stratosphere couplings tend to have important biases in the North Atlantic tropospheric jet [*Small et al.,* 2014], undermining the reliability of the simulated precipitation over WE.

In an attempt to systematize the connections between specific synoptic patterns and precipitation, classifications of daily synoptic patterns into weather types (WTs) are often performed [*Huth et al.,* 2008]. The European Cooperation in Science and Technology (COST) Action—COST733—was specifically devoted to the "Harmonisation and Application of Weather Type Classifications for European Regions" [*Huth*, 2010] and produced a catalog of WT classifications for 12 fixed European domains [*Philipp et al.,* 2010] using ERA-40 reanalysis. Classification schemes based on airflow direction/vorticity [e.g., *Lamb*, 1972; *Trigo and DaCamara*, 2000; *Pattison and Lane*, 2012; *Ramos et al.,* 2014a] or on cluster analysis [*Corte-Real et al.,* 1998; *Santos et al.,* 2005; *Chadee and Clarke*, 2015] are among the most common approaches. The performance of different WT classifications in discriminating, e.g., precipitation within a given sector, depends on the number of classes, target region, season, atmospheric parameters, and research focus [*Broderick and Fealy*, 2015]. However, *k*-means clustering based on MSLP is regarded as one of the best-performing classification schemes over western Europe [e.g., *Beck and Philipp*, 2010; *Casado et al.,* 2010; *Garcia-Valero et al.,* 2012; *Broderick and Fealy*, 2015].

Many studies have analyzed the relationships between WTs and precipitation in WE, namely, in the Iberian Peninsula [*Santos et al.,* 2005; *Fernandez-Montes et al.,* 2012; *Garcia-Valero et al.,* 2012], France [*Boe and Terray*, 2008; *Planchon et al.,* 2009], Ireland [*Broderick and Fealy*, 2015], Norway [*Tveito*, 2010], or over European-wide areas [e.g., *Jones and Lister*, 2009; *Beck and Philipp*, 2010; *Donat et al.,* 2010; *Hoy et al.,* 2014]. WTs have been also used as a diagnostic tool for model skill assessments and bias corrections [e.g., *Demuzere et al.,* 2009; *Pastor and Casado*, 2012; *Perez et al.,* 2014; *Photiadou et al.,* 2015]. Failure of climate models to accurately reproduce key patterns of synoptic variability can undermine their climate change projections [*Davini et al.,* 2014a].

Precipitation distribution and its extremes, inducing droughts and floods, are projected to change under future climate conditions in Europe, partially as a response to changes in large-scale atmospheric circulation [*Santos et al.,* 2007a; *Nikulin et al.,* 2011; *Seneviratne et al.,* 2012; *Sillmann et al.,* 2013b]. Although these future projections are in line with the observed past trends in precipitation and floods over Europe [*Madsen et al.,* 2014], their climate change signal is quite complex [*Greve and Seneviratne*, 2015] and requires further research. Taking into account the climate change projections for precipitation in WE, our main objectives are threefold: (1) to isolate WTs, defined on a daily basis, that can be used as a diagnostic tool of the large-scale mechanisms controlling precipitation over WE; (2) to evaluate the skill of state-of-the-art climate models in replicating the frequencies of occurrence of these WTs for recent climate conditions; and (3) to better understand the projected changes in precipitation over WE in light of the accompanying changes in WTs.

2. Data and Methods

As the main focus of the present study is on the westernmost European regions, the WT classification was carried out within a western European sector (30°W–10°E, 25–70°N), covering WE and adjacent water bodies. By targeting a sector that incorporates the main large-scale patterns governing precipitation over WE, the resulting WTs are also a meaningful diagnostic tool of the atmospheric circulation. The identification of WTs was carried out using daily MSLP fields over the period of 1979–2014 from ERA-Interim reanalysis [*Dee et al.,* 2011]. Other selected ERA-Interim daily atmospheric variables include the following: 500 hPa geopotential height (Z500), total precipitation, convective available potential energy (CAPE), zonal wind

component at 850 hPa (U850), 10 m horizontal wind components (zonal and meridional), and 500 hPa relative vertical vorticity (V500). All variables are defined at a spatial resolution of 0.75° longitude × 0.75° latitude. For validating ERA-Interim precipitation, two data sets of observation-based gridded precipitation were also used: (1) E-OBS daily precipitation, version 11.0, 0.25° regular grid [*Haylock et al.,* 2008] and (2) Global Precipitation Climatology Centre (GPCC) monthly precipitation, version 6.0, 0.5° regular grid, being 2010 the last available year [*Schneider et al.,* 2014].

For climate change assessments, an ensemble of 22 state-of-the-art global climate model runs (Table S1 in the supporting information), participating in the fifth phase of the Coupled Model Intercomparison Project —CMIP5 [*Taylor et al.,* 2012], is used. Daily precipitation, MSLP, and 850 hPa zonal wind for both recent past (1979–2005) and future (2071–2100) periods were retrieved. Recent past data were forced by historical greenhouse gas (GHG) concentrations, while data for the future period were forced by (Representative Concentration Pathways) RCP8.5 [*van Vuuren et al.,* 2011; *Intergovernmental Panel on Climate Change* (*IPCC*), 2013]. This scenario corresponds to a radiative forcing of 8.5 W m^{-2} by 2100, being the pathway comprising the highest GHG emissions [*Riahi et al.,* 2011]. This analysis was also carried out for RCP4.5 and for both scenarios over the 2041–2070 period. Given that results for RCP4.5 and 2041–2070 are generally very similar but with weaker signals to RCP8.5 over 2071–2100 (not shown), we focus here on the latter for the sake of succinctness.

For weather typing, seasonality at each grid point was removed from the raw MSLP fields. For that purpose, gridded long-term means were computed on a daily basis (1981–2010 baseline) and smoothed by 31 day moving averages. A principal component analysis was then applied as a preprocessing tool [*Wilks*, 2011], and only the 10 leading components were retained (~95% of explained variance). Lastly, a *k*-means clustering was applied to this subset of components, based on point-to-centroid squared Euclidean distances [*Wilks*, 2011]. Cluster seeding was carried out by preliminary clustering on a random 10% subsample, and the clustering algorithm was replicated 10 times. The solution with the lowest within-cluster variance was eventually selected. The discriminatory power, θ, of the WTs, i.e., their skill in separating daily precipitation totals at a given location, is calculated at specific locations. It is defined as $\theta = 1 - \mathrm{WSS/TSS}$, where WSS is the within-cluster sum of squares (squared deviations from cluster mean precipitation) and TSS is the total sum of squares (squared deviations from total mean precipitation), ranging from 0 (no discrimination) to 1 (maximum discrimination) [*Broderick and Fealy*, 2015]. Gridded (E-OBS and GPCC) monthly precipitation (predictand) is related to the monthly frequencies of occurrence of the WTs (predictors) by stepwise multivariate linear regressions, and the corresponding fractions of explained variance are estimated. Outliers are downweighted by robust fittings using bisquare weighting. The number of WTs corresponding to a stabilization of the area-mean explained variance over WE is chosen. As a sharp increase was found from two to five clusters, followed by a weaker increase up to eight clusters and a stabilization thereafter (not shown), we have chosen eight WTs. We aim at having the smallest number of physically meaningful WTs that optimally maximize the explained variance in monthly precipitation over WE (parsimony solution).

Owing to the different model grids, simulated data were bilinearly interpolated to the ERA-Interim grid (0.75° longitude × 0.75° latitude) within the WE sector (30°W–10°E, 25–70°N). The clustering on model outputs does not necessarily render the same WTs obtained from ERA-Interim. Hence, for the model outputs, a given day is keyed to the WT having the maximum spatial (point-by-point) Pearson correlation coefficient between that day MSLP and the WT composite from ERA-Interim (prototype correlation-based classification). This procedure warrants a common basis for the spatial configuration of the WTs ("frozen" patterns), and the differences between models and ERA-Interim can only be attributed to biases in the WT frequencies. To assess model performances, the sum of squared differences between the monthly mean frequencies in a given model and in ERA-Interim was computed. For each model, they are computed by WT for all months, by month for all WTs, or for a combination of the two (double-entry table). Skill scores are thus defined as the inverse of the sum of squares over the double-entry table normalized to unit maximum. This last measure enables ranking models in terms of their net ability to reproduce WT monthly mean frequencies. As unweighted ensemble means comprise less uncertainties than performance-based weighting [*Christensen et al.,* 2010], no weighting was applied herein.

3. Climate Change on Precipitation

The ERA-Interim annual mean precipitation pattern for the wider Euro-Atlantic sector shows a clear signature of the storm track over the North Atlantic, with a southwest-northeast tilted axis (Figure 1a). A noticeable

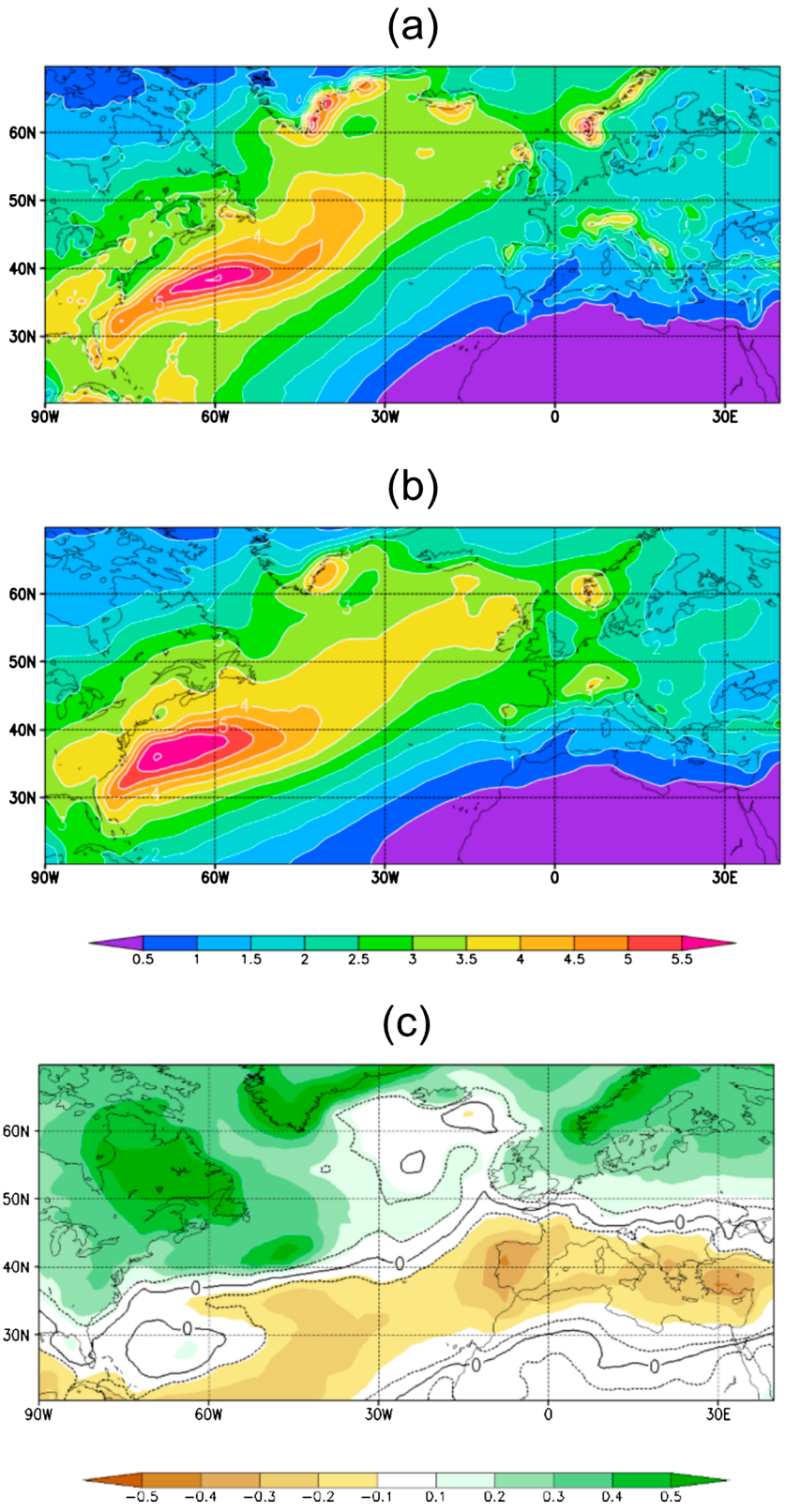

Figure 1. (a) ERA-Interim annual mean precipitation (in mm d^{-1}). (b) Ensemble mean annual mean precipitation (in mm d^{-1}) for 1979–2005. (c) Climate change signal (RCP8.5, 2071–2100 minus 1979–2005) of annual mean precipitation (in mm d^{-1}). Statistically significant changes at 95% confidence level are delimited by dotted lines.

maximum of ~6 mm d^{-1} is found over the western North Atlantic, close to the 40°N parallel. However, other maxima are found over Europe, namely, over southwestern Norway, southern Iceland, western Scotland, the Alps, and northwestern Iberia. Much drier conditions can be found over North Africa and the Mediterranean Basin. The very strong northwest-southeast contrast in precipitation amounts over the Iberian Peninsula is remarkable, suggesting strong orographic barrier effects on Atlantic air mass progression toward the Mediterranean Sea. Overall, the Atlantic-facing areas of WE are among the rainiest regions in Europe, as they are more exposed to the moist Atlantic winds and, when located on windward sides of mountain ranges, precipitation is further enhanced by orography-forced uplift of air masses.

The corresponding pattern from the CMIP5 model ensemble reveals a general good agreement with ERA-Interim, despite some differences in detail (Figure 1b). Models are thus able to capture the most important spatial features of mean precipitation within the Euro-Atlantic sector. With respect to their climate change signal on precipitation (2070–2100 minus 1979–2005), the opposite signs between northern and southern Europe, with zero line at 45–50°N, are the most striking features (Figure 1c). A strong increase of precipitation over Norway is accompanied by a strong decrease of precipitation over western Iberia (also over Greece and Turkey). Furthermore, the zero line presents its northernmost location over WE and depicts a large area with near-zero signal extending over the northeastern North Atlantic. Although these changes in precipitation were already reported by several studies [e.g., *IPCC*, 2013], their coherence with changes in the large-scale atmospheric circulation is not fully understood and needs further research. The weather typing approach will enable a more thorough dynamical interpretation of this climate change signal.

4. Weather Type Diagnosis

The clustering of the daily MSLP fields over the selected Euro-Atlantic sector leads to the identification of eight WTs. Their corresponding composite patterns in both the MSLP and Z500 highlight their main dynamical features in the large-scale atmospheric circulation (Figure 2), which will be described in section 4.2.

4.1. Occurrence and Seasonality

The WT monthly and annual mean frequencies of occurrence are shown in Figure 3. The WTs are named according to their seasonal prevalence. The three predominantly summertime and wintertime WTs are keyed as S1–3 and W1–3, respectively. The blocking-like types are keyed as B1–2 and occur less frequently in summer. The S1–3 types represent roughly 50% of the annual occurrences, whereas the W1–3 and B1–2 types represent, respectively, about 28% and 22%. S1 is the most frequent type (annual occurrence of 18%), followed by S3 (17%) and S2 (15%). W3 is the most frequent wintertime type (12%), while W1 is the least frequent (7%). The blocking types have similar occurrences (~11%). The WT monthly frequencies do not show statistically robust long-term trends in the period of 1979–2014 (not shown).

Regarding the WT seasonality (Figure 3), S1 occurrences peak in July (~40% of the days) and have their lowest occurrence in January (~5%). Although similar considerations can be made for S2 and S3, their seasonality is much less pronounced than for S1. This is particularly clear in the case of S3, for which occurrences of ~15% are found in January and of 20–25% in summer. Therefore, even though S3 is primarily a summertime WT, it is frequent throughout the year. The B1 occurrences show a bimodal distribution, peaking in May and October (15–20% of the days) and significantly lowering in summer and winter (transitional regime). B2, nevertheless, shows clear seasonality, with maximum occurrences in winter (~20%). W1–3 also reveal strong seasonality, but with minima in July and maxima in winter, though W1 also presents a second maximum in October. In winter, W1–3 have contributions ranging from 10 to 25%, whereas in summer they are infrequent ($<$1% for W2 in July). The most significant intertype transitional probabilities (cf. supporting information Figure S1) show important values for transitions from S2 to S1, and also from all the other WTs to the summertime types (S1–3), in line with their high recurrence (50% of all days).

4.2. Archetypal Spatial Patterns

As a typically summertime WT, the S1 pattern reveals a northeastwardly extended Azores high-pressure system, connected to a strong ridge over the eastern North Atlantic (Figure 2a). Subpolar low-pressure systems are relatively weak, as well as the meridional pressure gradients over the whole sector. In S2 there is a trough over northwestern Europe, accompanied by an Azores high close to its climatological location (Figure 2b).

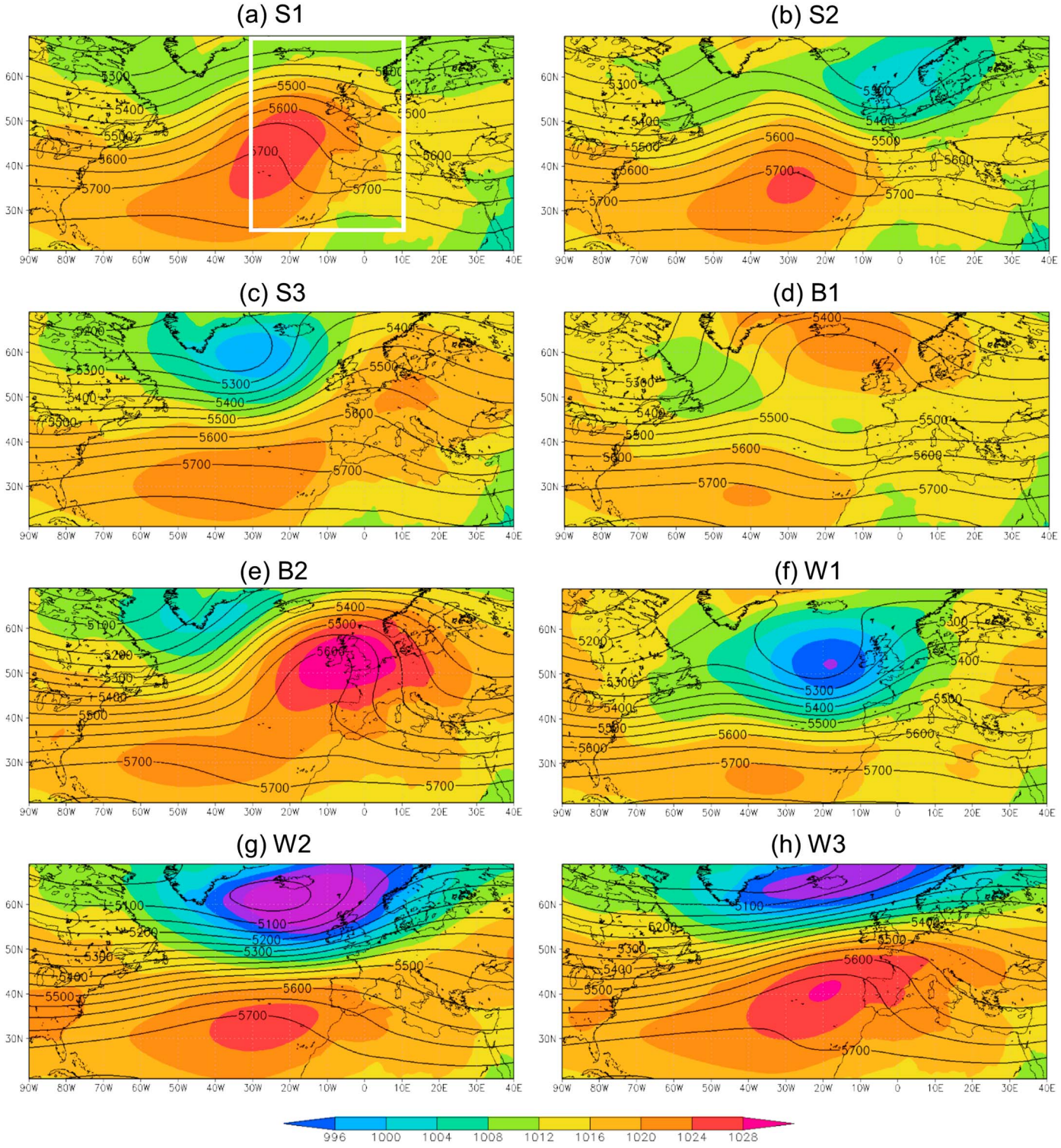

Figure 2. Composites of the mean sea level pressure (shading in hPa) and of the 500 hPa geopotential height (contours in gpm) for the eight outlined WTs over the period of 1979–2014 (ERA-Interim reanalysis). The sector used for weather typing (30°W–10°E, 25–70°N) is outlined by the white box in Figure 2a.

The resulting meridional geopotential gradient over WE is relatively strong. Two high-pressure systems are apparent in S3—the Azores high and the Central European high—shaping a high-pressure belt over most of Europe (Figure 2c). Weak Icelandic low-pressure systems are strongly blocked by this belt. A pronounced midtropospheric ridge (in Z500) over western and central Europe is also depicted.

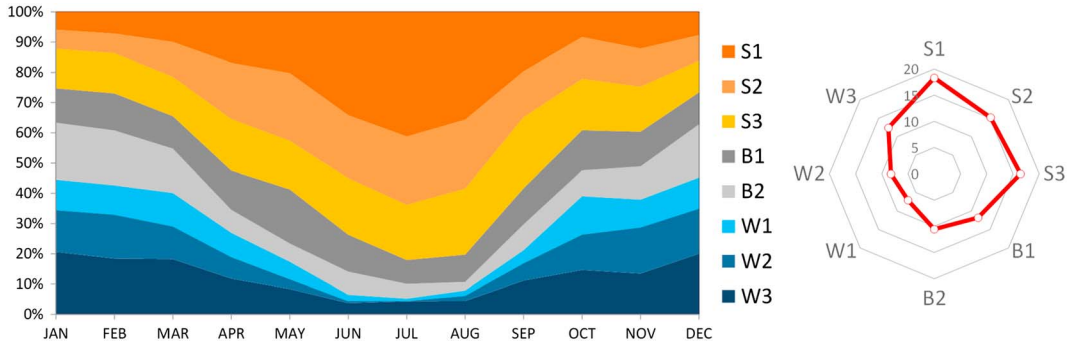

Figure 3. (left) Cumulative bar chart of the WT monthly mean relative frequencies of occurrence over the period of 1979–2014. (right) Corresponding WT annual mean frequencies of occurrence.

Regarding the blocking-like types, B1 is related to North Atlantic high-latitude blocking, with midtropospheric ridges and high-pressure systems extending over Iceland and Greenland (Figure 2d). The Azores subtropical high is southerly displaced, giving place to a zonal flow over the midlatitude North Atlantic. This inverted meridional pressure gradient over the eastern North Atlantic and WE is a typical blocking signature. B2 also features an inverted meridional pressure gradient (Figure 2e), but the blocking structure is southerly shifted (midlatitude blocking). The high-pressure core is located over the British Isles, associated with a very strong midtropospheric ridge over the eastern North Atlantic and WE.

With respect to the winter types, W1 is characterized by low-pressure systems just westward of the British Isles, though spreading their influence throughout WE (Figure 2f). A quite strong midtropospheric trough is also depicted for W1. In W2, the Azores high is relatively weak, while the Icelandic low is southerly displaced relatively to its climatological position (Figure 2g), resembling the NAO negative phase [*Hurrell*, 1995]. Conversely, W3 hints at a strong northeastwardly displaced Azores high, extending over southwestern and central Europe (Figure 2h). Deep Icelandic low-pressure systems are also displayed. Thus, W3 largely projects onto the NAO positive phase [*Hurrell*, 1995]. Although W2 and W3 present dipolar structures, with high pressures to the south and low pressures to the north, the W3 pattern is northeastwardly shifted with respect to W2 (Figure 5), and thus, their respective precipitation anomalies are nearly opposite (Figure 6).

4.3. Relations to Precipitation

The explained variances of monthly precipitation by WTs reveal an overall high agreement between the two precipitation data sets (E-OBS and GPCC) (Figure 4). WTs explain higher fractions of variance in the westernmost (Atlantic-facing) regions, which are more exposed to the direct Atlantic influences, such as southwestern Norway, Iceland, western Ireland, western Great Britain, Bretagne (France), and western Iberia.

The role played by each WT is not the same for each location. As an illustration, the empirical distributions of the daily precipitation for each WT and at four grid boxes (northwestern Iberia: 8.375°W, 42.125°N; Bretagne (France): 3.875°W, 48.375°N; western Scotland: 4.875°W, 56.875°N; and southwestern Norway: 5.625°E, 60.125°N) show significant regional differences (Figure 4). For northwestern Iberia W1, W2, B1, and S2 are the rainiest types, mostly W1, but with modest discriminatory power (26%), showing important spreading over the different types. For Bretagne, W1, W2, and S2 are the rainiest types (B1 is not as important as for northwestern Iberia), with high discrimination of precipitation (82%). For western Scotland, the distributions reveal a noticeable concentration of precipitation in W2 and W3 (70%), both of them related to strong westerlies over the region. Although W2 and W3 are also the rainiest types for southwestern Norway, there is considerable spreading (18%).

4.4. Dynamical Characterization

Composites of the zonal wind component at 850 hPa, fractions of "convective days" (herein defined as days having simultaneously CAPE $> 100\,\mathrm{J\,kg^{-1}}$ and negative omega vertical velocity), 10 m wind streamlines, 500 hPa relative vertical vorticity, and daily precipitation are used for a dynamical characterization of WTs (Figure 5). For S1, the eddy-driven jet is slight northerly shifted (note midlatitude negative anomalies) and southwesterly-northeasterly tilted (Figure 5a). These features are dynamically coherent with the strong anticyclonic ridge over the North Atlantic (Figure 2a). Additionally, the fraction of convective days is generally low,

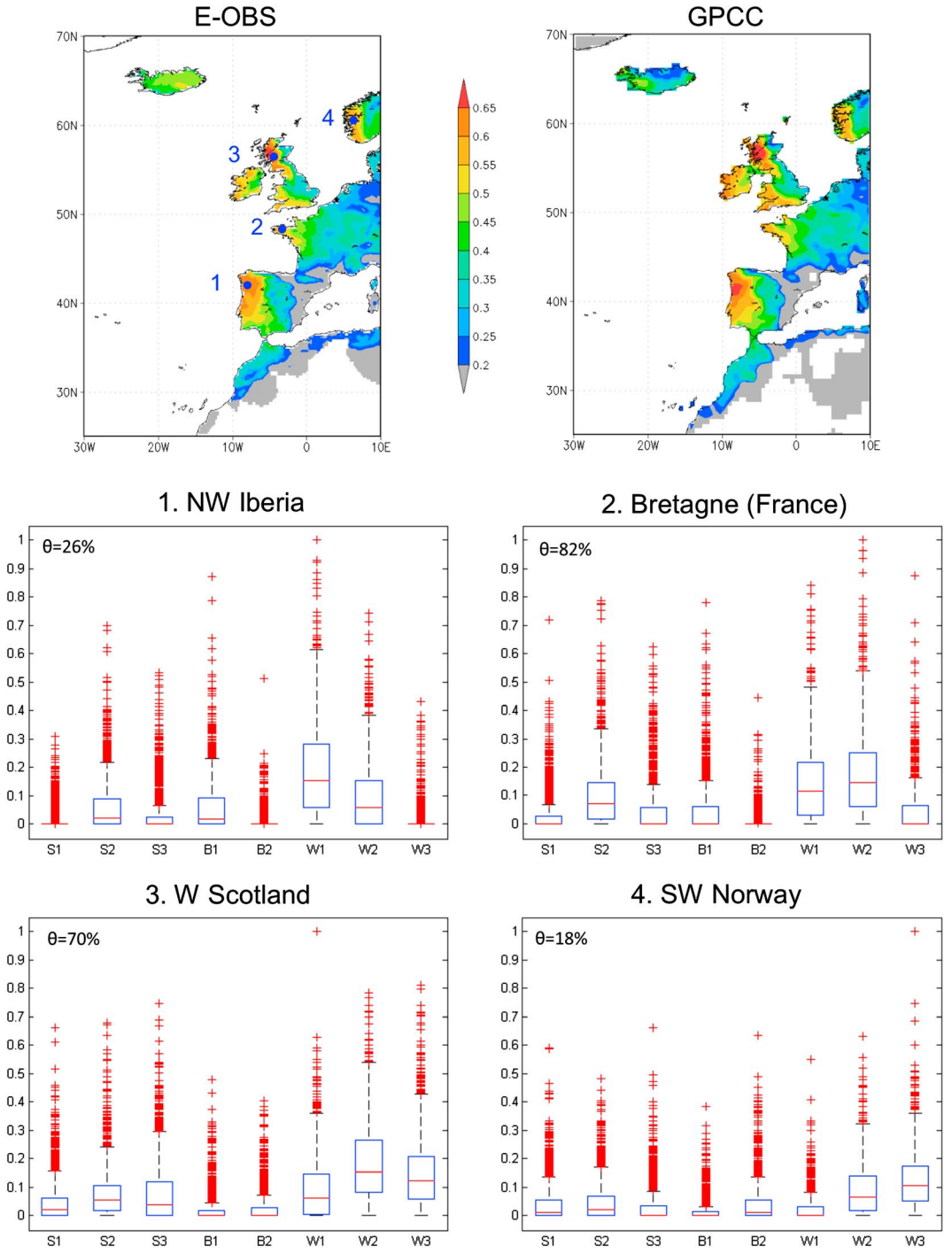

Figure 4. (top row) Fraction of explained variance of the monthly precipitation by the eight WTs ((left) E-OBS data set, version 11.0, 0.25° grid; (right) GPCC, version 6, 0.5° grid), estimated by stepwise multivariate regressions, over the western European sector and for the period 1979–2014 (E-OBS) or 1979–2010 (GPCC). (middle and bottom rows) Boxplot charts of the daily precipitation totals (normalized to unit maximum) associated with each WT over the period of 1979–2014 and for the four outlined locations: 1—northwest Iberia; 2—Bretagne (France); 3—western Scotland, and 4—southwest Norway (see top left panel and text for geographical coordinates). Medians are horizontal lines, upper (lower) box limits are the 75th (25th) percentiles, upper (lower) whiskers limits are nonoutlier maxima (minima) and "plus" symbols are outliers (absolute distance to median $> 1.5 \times$ interquartile range). The corresponding discriminatory powers (θ) at each location are also outlined.

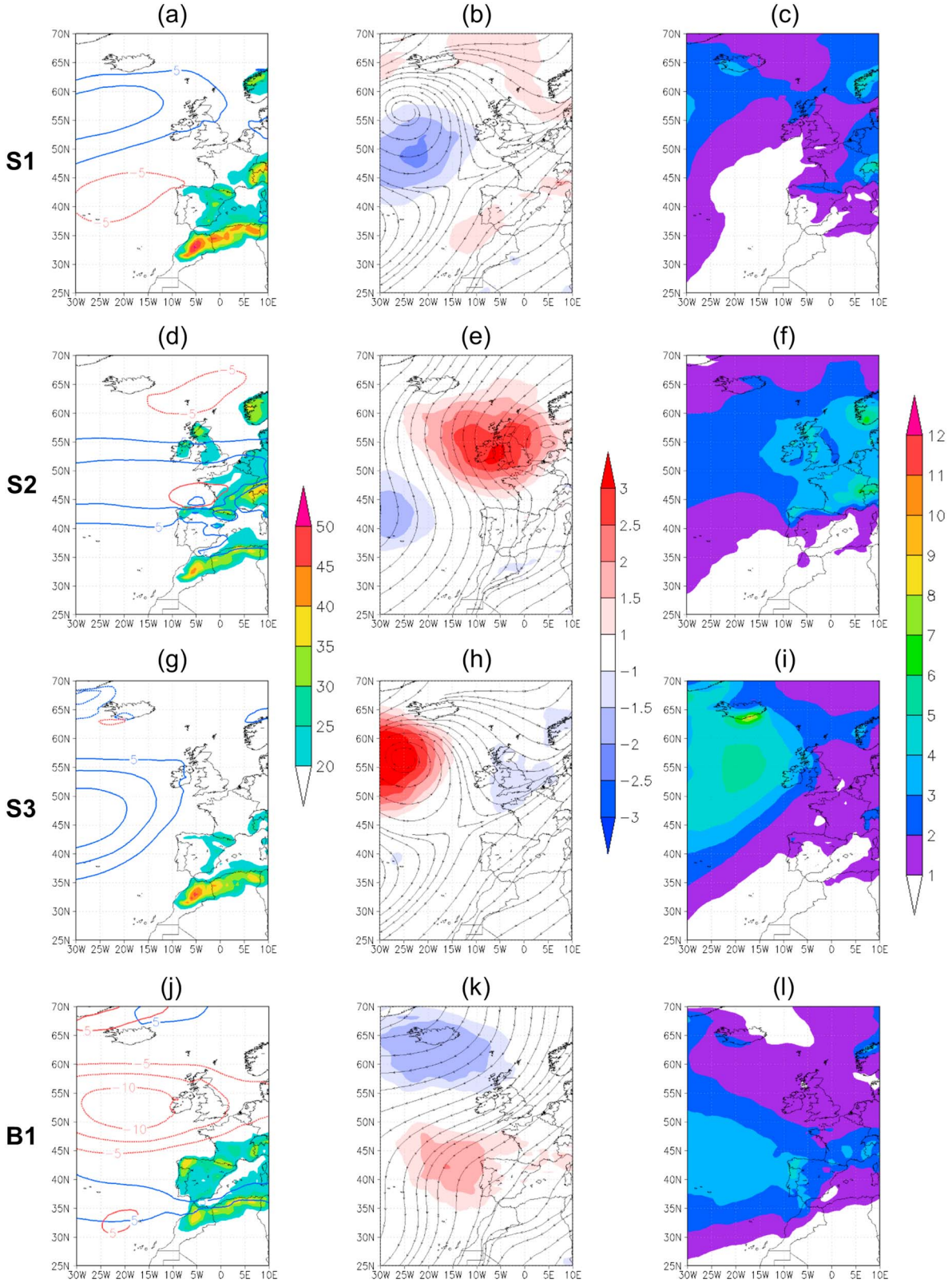

Figure 5. Composites for each WT over the period of 1979–2014 (ERA-Interim reanalysis) of the (first panel) zonal wind isotachs at 850 hPa (blue contours) and corresponding anomalies with respect to their baseline (1979–2014) annual means (red contours)—contours displayed at intervals of 2.5 m s^{-1} and omitted within the range −5 to 5 m s^{-1}—and fractions of convective days, i.e., days with CAPE > 100 J kg^{-1} plus negative omega vertical velocity in the 500–700 hPa layer (shading in %); (second panel) 10 m wind streamlines and 500 hPa relative vertical vorticity (shading in 10^{-5} s^{-1}); and (third panel) daily precipitation (in mm d^{-1}).

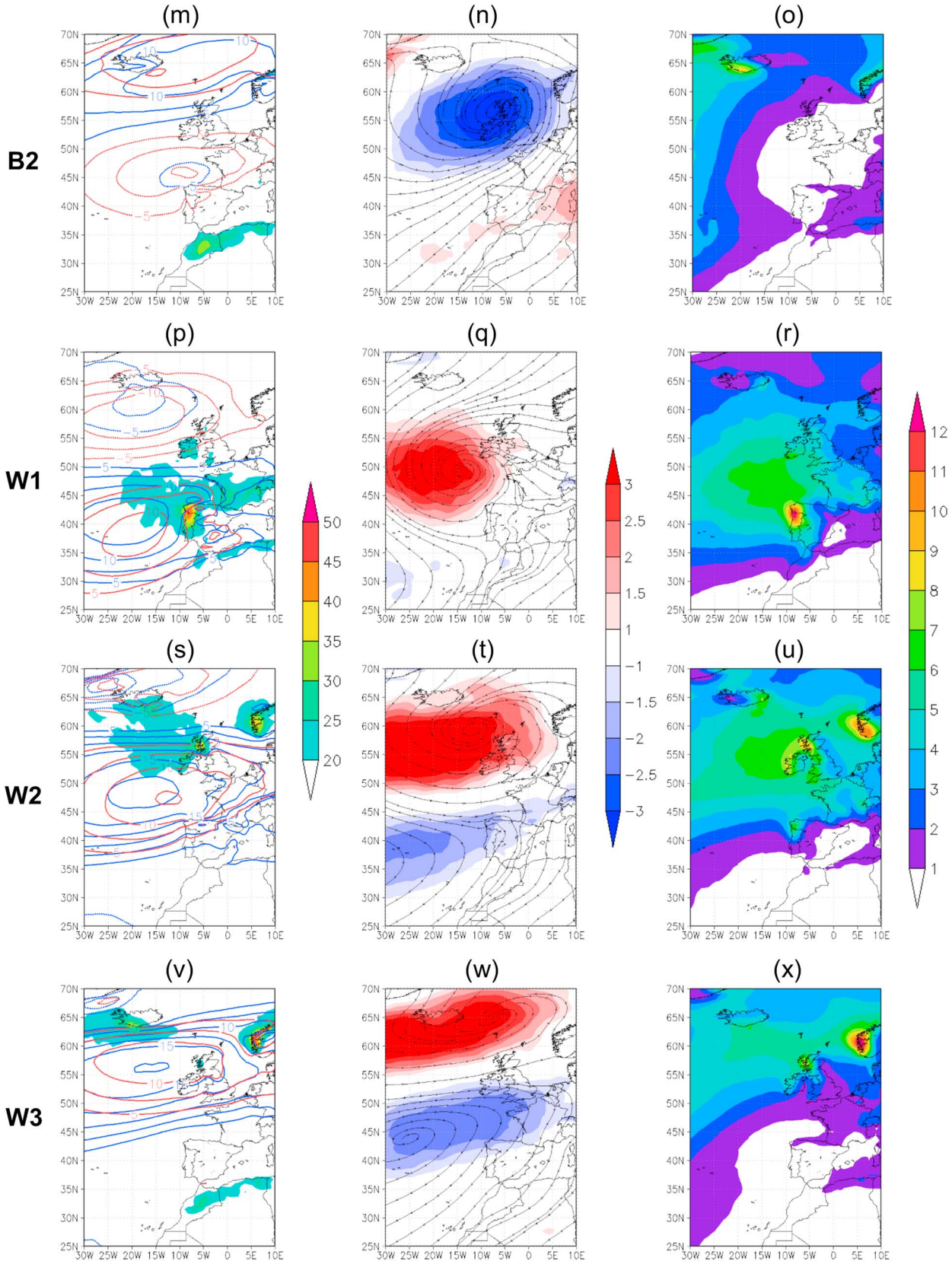

Figure 5. (continued)

apart from some mountainous regions, such as the Atlas range (North Africa) and the Alps, where some convective potential is observed (Figure 5a). The composites of the 10 m wind streamlines and of the 500 hPa vorticity hint at the anticyclonic circulation (clockwise rotation and negative vorticity, Figure 5b). Owing to its strong and wide anticyclonic ridge over the Euro-Atlantic sector (Figure 2a), S1 is commonly very dry over WE and the adjacent eastern North Atlantic (Figure 5c). Precipitation gradually increases eastward and northward in Europe, as the distance to the ridge axis increases. Relatively high precipitation amounts are recorded in southwestern Norway, which is far enough from the ridge and is thereby more exposed to westerly winds along its northern flank. Further, over the Cantabrian range (northern Spain) and the Pyrenees (Spain-France border), northerly winds lead to orographic barrier uplift of maritime air masses, thus triggering precipitation along northern Iberia and southwestern France. A similar reasoning can be applied to the Alps. Conversely, precipitation over oceanic and flat terrain areas is generally scarce.

The dynamical conditions of S2 are remarkably different from S1. The eddy-driven jet is predominantly zonal and covers most of WE (Figure 5d), with negative anomalies over Norwegian Sea and strong positive anomalies at ~45°N. The 10 m streamlines reveal prevailing northerly flow over WE but diverted by the cyclonic circulation over the British isles and the anticyclonic circulation over the midlatitude North Atlantic (Figure 5e). Significant precipitation occurs northward of the 40°N parallel (Figure 5f), generated by low-pressure systems developing over northern Europe (Figures 2b and 5e). Furthermore, in Europe, precipitation areas mostly coincide with areas with high frequency of convective days, emphasizing the importance of convection for precipitation occurrence (Figures 5d and 5f). Over North Africa and southern-eastern Iberia rainfall is scarce under S2.

For S3, the eddy-driven jet is significantly weakened as it approaches WE and is largely confined to the North Atlantic (Figure 5g), showing a near climate-mean pattern (neglectful anomalies). This is also in agreement with the high-pressure belt extending from the Azores to Eastern Europe (Figure 2c), which is also clear in both the near-ground airflow and the midtropospheric vorticity (Figure 5h). High precipitation amounts connected to low-pressure systems are found over the North Atlantic, but are blocked by the high-pressure belt over Europe, only reaching the westernmost areas of the British Isles and southwestern Norway (Figure 5i). Furthermore, precipitation tends to be largely related to frontogenesis/cyclogenesis, since the fraction of convective days is low over the rainiest areas under this circulation type (Figure 5g).

Regarding B1, a narrow belt of westerly winds at 850 hPa and along the 36°N parallel is a manifestation of low-pressure systems westward of Iberia (Figure 5j). Further, the significant negative anomalies in wind speed within the 45–60°N latitude range are a manifestation of the blocking structure (Figure 5j). Streamlines and vorticity hint at a common blocking-like structure (Figure 5k), with north negative and south positive vorticity cores over the eastern North Atlantic. B1 favors the occurrence of precipitation within a belt in between the Azores high and the high-latitude blocking high (Figures 2d and 5l). Under such circumstances, precipitation over WE is higher southward of the 47°N parallel. The recurrently high number of convective days suggests the important role played by convective mechanisms on precipitation over southwestern Europe (Figure 5j).

B2 also reveals a blocking-like configuration (Figures 2e and 5m) but southeasterly shifted by about 10° in latitude with respect to B1 (midlatitude blocking). The lack of convective potential over WE, along with the location of the eddy-driven jet poleward of 55–60°N, with easterly winds at 45°N, is noteworthy (Figure 5m). In fact, mean negative anomalies up to 10 m s^{-1} are depicted at midlatitudes, while anomalously strong winds are observed at high latitudes, both attesting the presence of strong blocking structures. These dynamical features are also accompanied by very strong anticyclonic circulation over the British Isles (Figure 5n), which favors air mass subsidence. Therefore, mean daily precipitation is inferior to 2 mm over WE, with the most notable exception for southwestern Norway, where mean daily precipitation exceeds 5 mm (Figure 5o). Overall, B2 is the driest regime over WE (Figure 4).

For W1 baroclinicity might be a determinant for precipitation occurrence, taking into account the southerly displaced eddy-driven jet (anomalously strong/week wind speeds equatorward/poleward of 45°N), with remarkably strong westerlies over southwestern Europe (Figure 5p). The presence of strong cyclones over the midlatitude North Atlantic is corroborated by the streamlines and the vorticity pattern (Figure 5q). These strong low-pressure systems (Figure 2f), developing nearby or over WE, potentiate high precipitation amounts across the whole region (Figure 5r). This is particularly clear over northwestern Iberia, where rain-generating conditions, promoted by frontal systems and strong southwesterly winds, are reinforced by convection (Figure 5p) and orographic uplift on the windward sides of mountain ranges. The remarkable

contrast between the Atlantic-facing and the Mediterranean-facing Iberia reflects the key role of the consecutive orographic barriers on the rain-generating processes. Indeed, in northwestern Iberia, the rainiest conditions occur for this WT (cf. Figure 4).

For W2, the anomalously strong westerlies over most of WE reflect the propagation and development of baroclinic waves (Figure 5s). Streamlines and vorticity suggest strong cyclogenesis at higher latitudes in the North Atlantic and WE (Figure 5t). Convection is important over Scotland and southwestern Norway, areas close to the low-pressure core, but of secondary relevance in other regions (Figure 5s). The heaviest precipitation occurs over northwestern Europe (Figure 5u) in association with the passage of strong subpolar cyclones and frontal systems. Conversely, the western Mediterranean, largely sheltered by orography (leeward side), is the driest area (Figure 5u).

The enhanced Azores high in W3 diverts the baroclinic waves to northern Europe and the Norwegian Sea (Figures 2h and 5v). The core of an anomalously strong eddy-driven jet is located along the 55°N parallel (Figure 5v), clearly northward of its locations in W1 and W2. The strong north-south contrast in the dynamical conditions over the Euro-Atlantic sector is emphasized by both the near-surface streamlines and the midtropospheric vorticity (Figure 5w). Hence, mean daily precipitation exceeds 9 mm in Scotland and southwestern Norway, with important convective potentials (Figure 5v), whereas in regions southward of 45°N the mean daily precipitation is inferior to 3 mm and most of Iberia experience no rainfall (Figure 5x). In fact, after B2, W3 is the second driest WT over southwestern Europe.

An overall good agreement between ERA-Interim and E-OBS precipitation was found for each WT (Figures 5 and S2), which is an important validation of the linkages between WT and precipitation. The grid point ratios between mean precipitation for each WT and the corresponding climate-mean precipitation are shown in Figure 6. These rates confirm that S1 and B2 are the driest types throughout WE. S3 is generally dry, while W3 is also dry apart from Norway and Scotland. W1 and W2 are very wet over most of Iberia and the British Isles, respectively. B1 displays a north-south contrast, being wet/dry over southern/northern WE.

5. Climate Change on Weather Types Versus Precipitation

5.1. Model Skill in Reproducing Large-Scale Circulation

CMIP5 models are used to assess WT frequencies for recent and future climate conditions and to relate projected changes in WT to precipitation changes. First, the ability of models to replicate WTs is evaluated. Skill scores (cf. section 2) reveal high intermodel variability (Figure S3). The most skillful model is CMCC-CM (note its highest horizontal resolution, Table S1), followed by MPI-ESM-LR and MPI-ESM-MR, also in agreement with previous studies [e.g., *Perez et al.,* 2014]. The IPSL-CM5B-LR, with a relatively coarse grid, presents the lowest skill, followed by FGOALS-g2.

A more detailed description of the discrepancies between models and observations can be found either by WT (Table S2) or by calendar month (Table S3). Differences in the annual mean frequencies by model run and WT are shown in Table S4. The low skill of IPSL-CM5B-LR is related to a strong overestimation of the frequencies of occurrence of B1 in summer (frequencies of occurrence of roughly 80% in June and July, not shown) and with an underestimation of the summertime types (S1–S3) and of the W3 type. Regarding FGOALS-g2, a similar limitation is detected with B1 in summer but with lower discrepancies (up to 41% in July, not shown). The frequencies of W1 in winter are also largely overestimated by this model (up to 40% in November, not shown). For the remaining models, smaller misrepresentations of the WT seasonality are identified. Otherwise, most models overestimate the frequencies of occurrence of W1 and W2 while underestimating the occurrences of B1, B2, S1, and S3 (Table S4). These outcomes suggest an overestimation of zonal airflow WTs and an underestimation of WTs associated with strong ridges/troughs, i.e., strong disturbances to the zonal mean flow. This is indeed a well-documented shortcoming of climate model simulations over the North Atlantic [e.g., *Barnes and Polvani*, 2013; *Cattiaux et al.,* 2013].

5.2. Future Projections of WT Frequencies

WT frequencies are now assessed under RCP8.5 for 2071–2100. Compared to recent climate conditions, significant changes in WT frequencies are revealed (Figures 7 and 8). At the annual time scale (Figure 7a), the dry S1 type is projected to become more frequent (ensemble average increase of 4.4%). Despite important intermodel variability, all models agree with a more frequent S1 type under future climate conditions. W1,

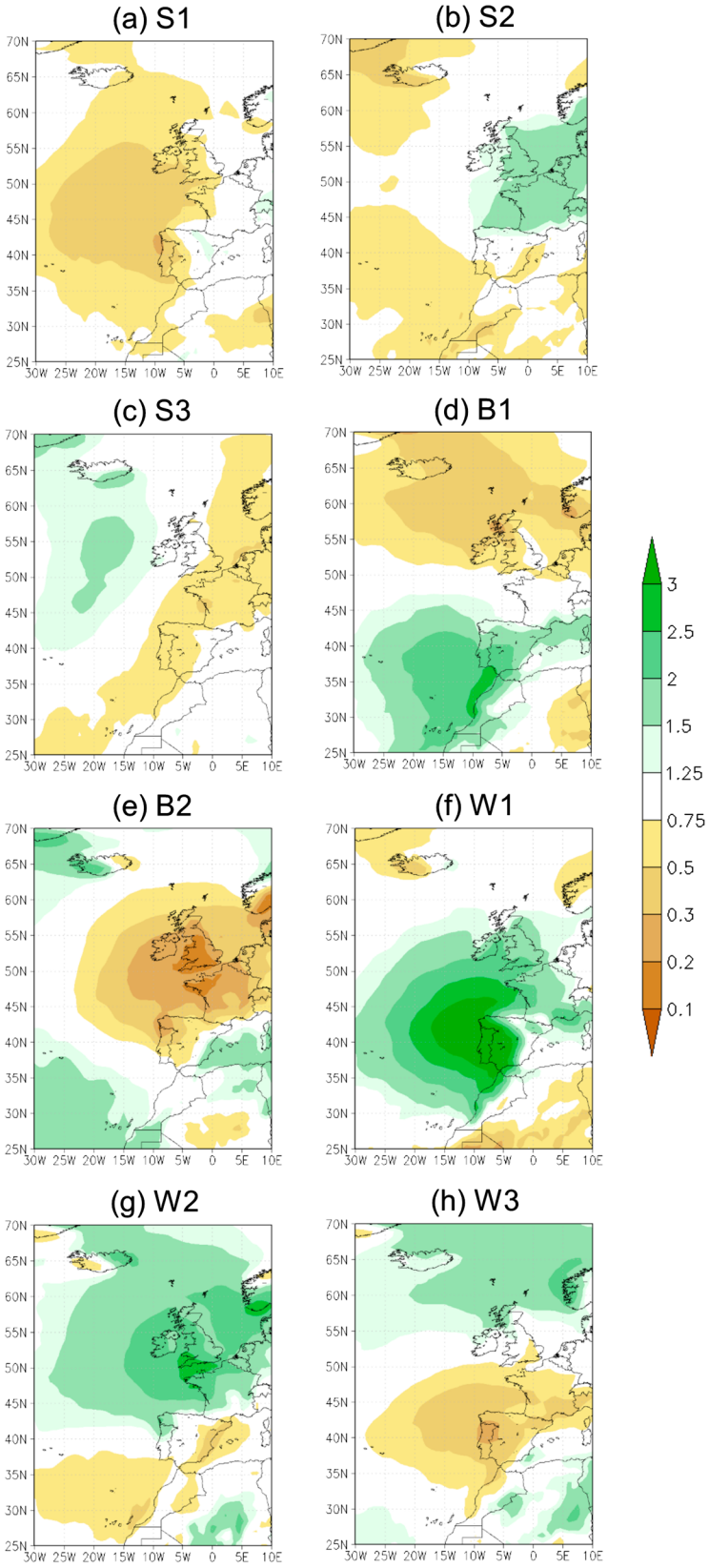

Figure 6. Ratios between mean precipitation for each WT and climate-mean precipitation (in mm d^{-1}) over the period of 1979–2014 (ERA-Interim). Note that the scale is not uniform.

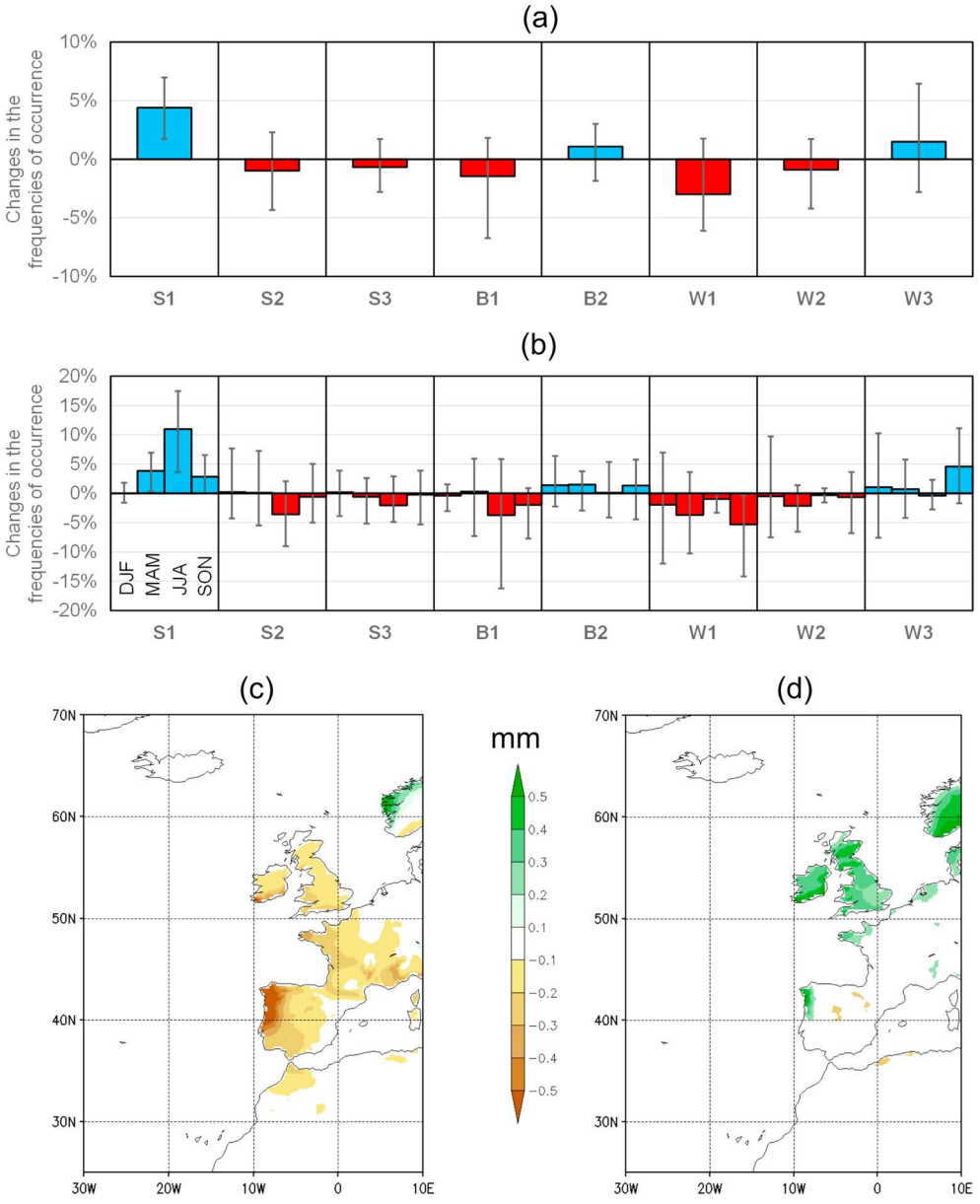

Figure 7. (a) Ensemble mean climate change signal (RCP8.5, 2071–2100 minus 1979–2005) of the annual frequencies of occurrence of the eight WTs (equally weighted 22 member ensemble). Maxima and minima for each WT are outlined by whiskers. (b) The same as in Figure 7a but for the December–February (DJF), March–May (MAM), June–August (JJA), and September–November (SON) frequencies of occurrence. (c) Climate change signal associated with the changes in Figure 7a, estimated by a regression analysis and using E-OBS precipitation over 1979–2014 for model calibration. (d) Differences between the multimodel ensemble and WT-derived climate change signals of annual mean precipitation (Figures 1c–7c).

which is particularly relevant for precipitation over southwestern Europe, is projected to become less frequent (−3%). There is also a wide agreement among models concerning this outcome, as only MRI-ESM1 projects a slight increase in W1 frequency. Despite the higher uncertainty (lower agreement) for the other WTs, multimodel ensemble means have proven higher skills than for each model separately [*Sillmann et al.,* 2013a]. Ensemble means reveal that B2 and W3 are likely to become more frequent, while S2, S3, B1, and W2 are projected to become less frequent (Figure 7a). The strong increase in the frequency of S1 is particularly noteworthy in summer (June-July-August (JJA)), while the decrease in W1 is stronger in spring (March-April-May (MAM)) and particularly in autumn (September-October-November (SON)) (Figure 7b). The projected seasonal changes for the other WT largely agree with the annual changes (Figure 7b). The seasonal changes also highlight a widening of S1 typical summertime conditions to spring and autumn.

RCP8.5 2071–2100	S1	S2	S3	B1	B2	W1	W2	W3
BCC-CSM1	3.7%	−0.6%	−0.1%	−1.0%	1.1%	−3.4%	−2.2%	2.6%
BCC-CSM1-m	5.0%	0.2%	−1.6%	−1.3%	−0.2%	−3.0%	−0.3%	1.2%
BNU-ESM	4.2%	−4.3%	−0.9%	1.8%	1.7%	−4.4%	−1.4%	3.3%
CanESM2	4.7%	1.0%	−2.1%	0.6%	−0.5%	−2.0%	−2.9%	1.2%
CMCC-CESM	3.2%	0.7%	−1.0%	−1.3%	−1.9%	−1.7%	0.7%	1.3%
CMCC-CM	2.6%	−0.5%	−1.1%	−2.7%	1.1%	−1.3%	0.1%	1.9%
CMCC-CMS	2.8%	−0.3%	1.1%	−1.9%	1.4%	−4.1%	0.5%	0.4%
CNRM-CM5	3.8%	−2.2%	−0.5%	0.0%	2.3%	−1.0%	−1.6%	−0.8%
FGOALS-g2	5.2%	0.8%	0.5%	−4.8%	0.6%	−4.9%	1.7%	0.9%
GFDL-ESM2G	4.4%	−1.7%	−0.6%	−1.9%	1.9%	−5.0%	−2.0%	4.8%
HadGEM2-AO	6.7%	−1.7%	0.2%	0.7%	3.0%	−2.6%	−4.2%	−2.1%
HadGEM2-CC	6.6%	−2.4%	−2.5%	0.7%	1.7%	−2.3%	−1.8%	−0.1%
IPSL-CM5A-MR	6.2%	1.3%	−1.1%	−3.7%	−0.5%	−2.3%	−0.9%	1.0%
IPSL-CM5B-LR	4.2%	2.3%	0.4%	−6.7%	1.9%	−4.6%	1.1%	1.4%

Figure 8. Climate Change Signal (RCP8.5, 2071–2100 Minus 1979–2005) in the Frequencies of Occurrence of Each WT and for Each Model Run (for the Expansions of Abbreviations and Acronyms See http://www.ametsoc.org/PubsAcronymList). Cell shading ranges from heavy blue (minimum) through white (0%) to heavy red (maximum). Ensemble means are also shown.

5.3. Discussion of WTs Versus Precipitation Changes

The increase in the occurrence of the driest WTs (S1, B2, and W3), featuring northerly displaced (with respect to their climate-mean pattern) high-pressure systems within the Euro-Atlantic sector (Figure 2), is corroborated by previous studies using CMIP5 models [e.g., *Davini et al.,* 2014b; *Belleflamme et al.,* 2015]. Moreover, these WTs are characterized by a poleward shifted eddy-driven jet with respect to its annual mean latitude (Figures 5a, 5m, and 5v). In fact, the coupling between enhanced midlatitude anticyclonic conditions and the poleward displacement of jets has been demonstrated by previous studies [*Barnes and Polvani*, 2013; *Zappa et al.,* 2015]. As the jet and the associated storm tracks shift poleward, precipitation over northern/southern Europe tends to increase/decrease [*Zappa et al.,* 2014]. On a seasonal basis, the climate change signals on both precipitation and jet reveal a good correspondence (Figure S4). The robust decreases of summer precipitation within the 45–50°N belt (note that precipitation southward of it is already very scarce) and of spring/autumn precipitation over western Iberia are particularly striking changes. For winter, the jet stream shows rather an eastward extension over Europe, resulting in a different pattern of change for precipitation (Figure S4). These outcomes are also in accordance to recent past changes in both WT frequencies and observed precipitation trends over Europe [*Hoy et al.,* 2014].

The increase in the occurrence of the two driest WTs (S1 and B2) is expected to contribute to an overall decrease in precipitation over WE (Figures 6a and 6e). Conversely, the increase in W3 occurrence contributes to an increase in precipitation over the northernmost regions, such as Norway (Figure 6h). The reduced frequency of W1 significantly affects the southern half of WE, particularly western Iberia (Figure 6f). Despite the smaller magnitude, the same applies to B1 (Figure 6d), strengthening the previous signal. Further, the decrease in S2 and W2 frequencies contributes to reduced precipitation amounts over most of WE (Figures 6b and 6g). Finally, the decrease in S3 frequencies leads to lower precipitation over the northeastern North Atlantic (Figure 6c).

The joint contribution of the changes of WT frequencies to the precipitation change can be quantified under the assumption that the observed statistical relationships between WTs and precipitation remain invariant

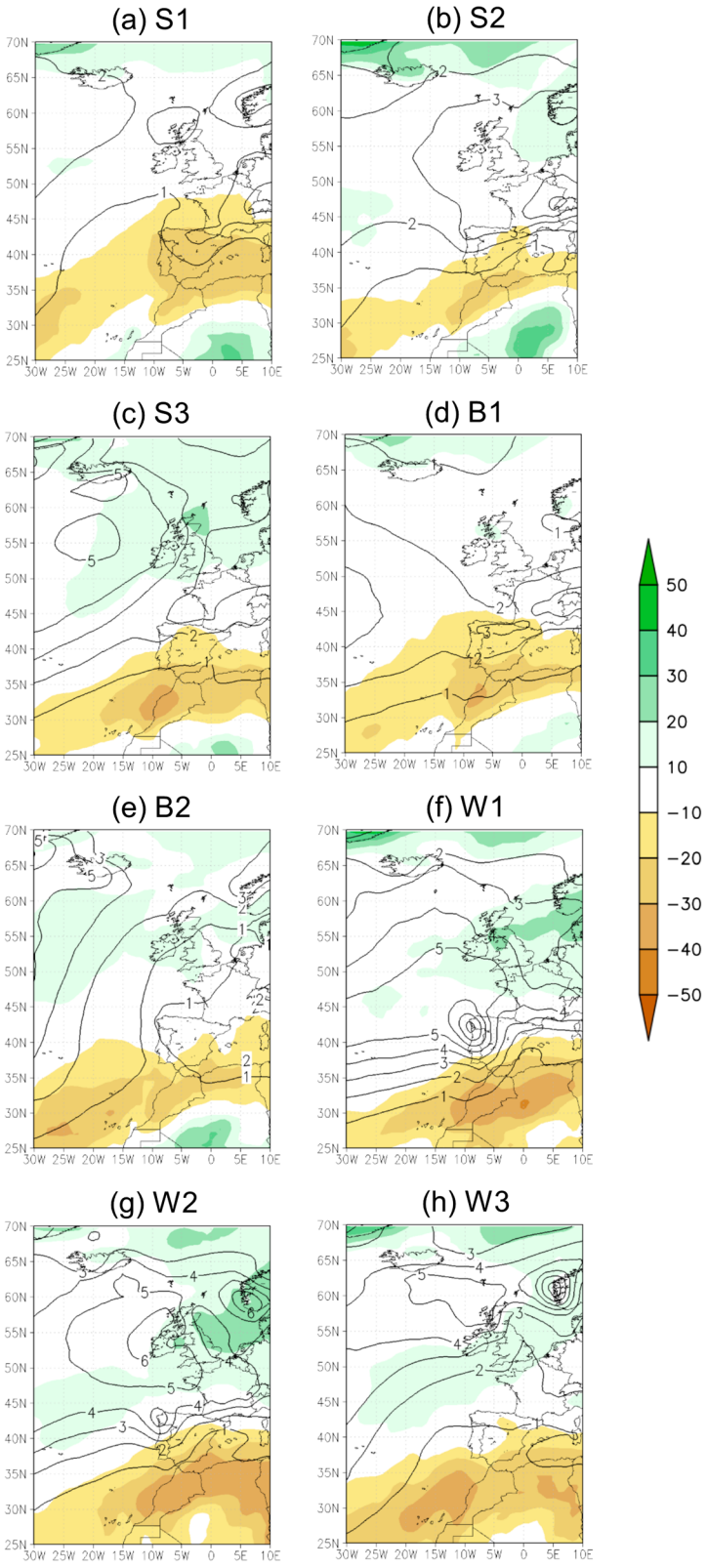

Figure 9. Ensemble mean daily precipitation for 1979–2005 (contours in mm d^{-1}) and relative future variations (2071–2100 versus 1979–2005) of precipitation (shading in %) for each WT. Changes not statistically significant at 95% confidence level are white shaded.

under future climate conditions. For that purpose, the previous regression equations between monthly WT frequencies (predictors) and E-OBS monthly precipitation (predictand) for 1979–2014 (Figure 4) are used. As GPCC ends in 2010 and has lower spatial resolution, E-OBS will be preferred for this analysis. The results reveal widespread decreases in annual mean precipitation, with the exception of Norway (Figure 7c). Furthermore, there is high agreement between this pattern and the ensemble mean change in precipitation over western Norway and Iberia (Figures 1c and 7c). On the other hand, a slight decrease in annual precipitation is depicted over the British Isles and southern Norway, unlike the projected increase derived directly from the CMIP5 models (Figures 1c and 7c). For comparison purposes, the pattern for the ensemble mean climate change signal of annual precipitation (Figure 1c) was bilinearly interpolated to the E-OBS grid (0.25°). The WT-derived climate change signal (Figure 7c) was then subtracted from the simulated climate change signal (Figure 1c). The resulting pattern depicts the changes not directly explained by the WTs (Figure 7d), confirming that the most notable discrepancies are found over the northern parts of the domain, namely, the British Isles and southern Norway (Figure 7d). The slightly different locations of the negative anomaly cores over western Iberia (Figures 1c and 7c), possibly owed to the different spatial resolutions of the data sets, may explain the differences along the north-western coast. Still, the climate change signals for annual precipitation are largely coherent.

This disagreement motivates a more detailed analysis. In fact, changes in the ensemble mean daily precipitation for each WT are noteworthy (Figure 9). It is striking that all WTs feature an increase in precipitation northward of 45–50°N and a decrease southward, with some variations, disclosing high resemblance with changes projected for the annual means (Figure 1). This WT-independent background climate change signal in precipitation intensity strengthens the north-south contrast in precipitation over WE and explains the discrepancies between simulated precipitation changes and WT-derived changes (Figures 1c and 7c).

Two factors can underlie the WT-independent signal: (i) changes in the precipitation-generating mechanisms (extrapolation of WT-precipitation relations to the future) and/or (ii) systematic model biases. For the first factor, alterations in thermodynamic processes may play a critical role, since the dynamical characteristics are fundamentally unchanged under each WT. In fact, previous studies suggested that global warming can modify the circulation patterns associated with precipitation in Europe [*Huth et al.,* 2008; *Belleflamme et al.,* 2015], not only their frequencies but also their underlying mechanisms. Concerning model biases, since the WT-precipitation relations are obtained from observation-based data sets (ERA-Interim versus E-OBS), models may not accurately reproduce these relationships. Furthermore, models tend to exacerbate flow zonality over the Euro-Atlantic sector (section 5.1), overestimating the frequencies of zonal airflow WTs, which are generally favorable to precipitation over the British Isles. Conversely, the frequencies of WTs related to strong ridges/troughs, leading to strong axially asymmetric anomalies, are often underestimated. In fact, the simulated precipitation changes are strongly zonal over WE (Figure 1c), as well as the changes in daily mean precipitation for each WT (Figure 9). This might be an artifact resulting from the overestimation of airflow zonality by most models. A few models (e.g., HadGEM2-AO) do project a decrease in precipitation over the British Isles and high-latitude eastern North Atlantic (not shown). Although further research is needed to test these two hypotheses, these important caveats need to be taken into consideration when interpreting precipitation projections for WE.

6. Summary and Conclusions

Multimodel ensemble climate change projections for precipitation over WE suggest significant drying trends over southern Europe and enhanced precipitation over its northern areas. In order to improve our current understanding of the driving dynamical mechanisms of these changes, an innovative weather type classification within a North Atlantic-western European sector (30°W–10°E, 25–70°N) is developed. Eight circulation types, with conspicuous seasonality and clearly distinct synoptic conditions, are identified: S1, S2, S3 (typical summertime types), W1, W2, W3 (typical wintertime types), B1, and B2 (blocking-like types). The relationships between WTs and precipitation variability over western Europe indicate their high relevance in discriminating precipitation on both daily and monthly time scales, particularly in the Atlantic-facing regions.

The selected geographical sector allows the inclusion of most of the large-scale dynamical features associated with midlatitude weather and climate variability over the eastern North Atlantic and WE. The selection of a region comprising the relevant precipitation-generating atmospheric flow for WE is a clear advantage over previous classifications carried out for either narrow sectors (e.g., only covering the British Isles or the Iberian Peninsula)

or large sectors (e.g., covering the whole of the North Atlantic and Europe). This new circulation catalog, and the links to precipitation over WE, can be used not only as a diagnostic tool of atmospheric circulation modulating precipitation over WE but also in statistical-dynamical downscaling applications [e.g., *Fuentes and Heimann*, 2000; *Sousa et al.,* 2013].

Using WTs as a diagnostic tool, the ability of 22 CMIP5 models to represent their frequencies over a recent past (1979–2005) was first analyzed. Some significant biases are identified, suggesting model limitations in simulating the North Atlantic large-scale atmospheric circulation, mostly by underestimating zonally asymmetric WTs, such as those featuring strong ridges or blocking-like structures. Under future climate conditions (2071–2100), following RCP8.5, an increase in the frequencies of occurrence of S1, B2, and W3 (the three driest WTs) is found, together with a decrease in the occurrence of the rainiest WTs, particularly W1. These findings are in line with a poleward shift of the eddy-driven jet over the North Atlantic on annual average, triggering an overall decrease/increase of annual precipitation southward/northward of 50°N. A considerable part of this signal can be explained by changes in WT frequencies. However, a mismatch is identified over the British Isles and southern Norway, where the projected ensemble precipitation trend and the estimated trend based on the changes in WT frequencies alone are dissimilar. A WT-independent background signal, with an increase (decrease) in precipitation over northern (southern) WE, underlies these discrepancies. Potential drivers of this WT-independent signal are (i) alterations in precipitation-generating thermodynamic processes under future climate conditions, related to, e.g., higher temperatures, enhanced latent heat release, and moisture content at lower levels and (ii) model systematic bias, such as overestimation of zonal flow over the Euro-Atlantic sector. While we speculate that a combination of these two factors may be the most probable potential driver of the WT-independent background signal, a more detailed analysis is left for future work. In line with previous studies [e.g., *Sillmann et al.,* 2013b], the present results provide further evidence of the advantages of considering multimodel ensembles to obtain robust estimates of climate change signals. This advantage owes partially to the cancelation of systematic errors between individual model simulations, which can be attributed to a variety of misrepresentations of the physical mechanisms underlying climate variability and change. In fact, multimodel ensembles have been shown to consistently outperform individual model experiments for different atmospheric fields and spatial domains [e.g., *Gleckler et al.,* 2008].

The low skills of some CMIP5 models to properly replicate the observation-based WTs indicate the need for model improvements in simulating the large-scale circulation over the Euro-Atlantic sector. Since precipitation over WE is largely governed by these WTs, the reliability of precipitation projections for future climates over WE is strongly dependent on the model ability to realistically simulate their underlying mechanisms, including the ability to reproduce the location and/or strength of the midlatitude eddy-driven jet. Therefore, future research should focus on these model limitations, contributing to lower the uncertainties in climate change projections for WE. A reduction on uncertainties related with precipitation projections would be beneficial for a wide range of climate change impact assessments, ranging from hydrology (e.g., water supply and management) and energy (e.g., hydroelectric power generation and renewable energy resources) to agri-forestry systems (water stress on crops and irrigation) and environment (air/water quality, biodiversity, and sustainability of ecosystems).

Acknowledgments

This work is supported by European Investment Funds FEDER/COMPETE/POCI–Operacional Competitiveness and Internacionalization Programme, under the project POCI-01-0145-FEDER-006958, National Funds by FCT-Portuguese Foundation for Science and Technology, under the project UID/AGR/04033, and by the project "ModelVitiDouro"—PA 53774, funded by the Agricultural and Rural Development Fund (EAFRD) and the Portuguese Government by Measure 4.1—Cooperation for Innovation PRODER program—Rural Development Programme. We acknowledge the E-OBS data set from the EU-FP6 project ENSEMBLES (http://ensembles-eu.metoffice.com) and the data providers in the ECA&D project (http://www.ecad.eu). We also thank the Coupled Model Intercomparison Project Phase 5 (CMIP5) for supplying the climate model data. We are also thankful to the two anonymous reviewers for their valuable comments and suggestions.

References

Andrade, C., J. A. Santos, J. G. Pinto, and J. Corte-Real (2011), Large-scale atmospheric dynamics of the wet winter 2009–2010 and its impact on hydrology in Portugal, *Clim. Res.*, *46*(1), 29–41, doi:10.3354/cr00945.

Barnes, E. A., and L. Polvani (2013), Response of the midlatitude jets, and of their variability, to increased greenhouse gases in the CMIP5 models, *J. Clim.*, *26*(18), 7117–7135, doi:10.1175/JCLI-D-12-00536.1.

Barnston, A. G., and R. E. Livezey (1987), Classification, seasonality and persistence of low-frequency atmospheric circulation patterns, *Mon. Weather Rev.*, *115*(6), 1083–1126, doi:10.1175/1520-0493(1987)115<1083:CSAPOL>2.0.CO;2.

Beck, C., and A. Philipp (2010), Evaluation and comparison of circulation type classifications for the European domain, *Phys. Chem. Earth*, *35*(9–12), 374–387, doi:10.1016/j.pce.2010.01.001.

Belleflamme, A., X. Fettweis, and M. Erpicum (2015), Do global warming-induced circulation pattern changes affect temperature and precipitation over Europe during summer?, *Int. J. Climatol.*, *35*(7), 1484–1499, doi:10.1002/joc.4070.

Boe, J., and L. Terray (2008), A weather-type approach to analyzing winter precipitation in France: Twentieth-century trends and the role of anthropogenic forcing, *J. Clim.*, *21*(13), 3118–3133, doi:10.1175/2007JCLI1796.1.

Broderick, C., and R. Fealy (2015), An analysis of the synoptic and climatological applicability of circulation type classifications for Ireland, *Int. J. Climatol.*, *35*(4), 481–505, doi:10.1002/joc.3996.

Casado, M. J., M. A. Pastor, and F. J. Doblas-Reyes (2010), Links between circulation types and precipitation over Spain, *Phys. Chem. Earth*, *35*(9–12), 437–447, doi:10.1016/j.pce.2009.12.007.

Casanueva, A., C. Rodriguez-Puebla, M. D. Frias, and N. Gonzalez-Reviriego (2014), Variability of extreme precipitation over Europe and its relationships with teleconnection patterns, *Hydrol. Earth Syst. Sci.*, *18*(2), 709–725, doi:10.5194/hess-18-709-2014.

Cattiaux, J., H. Douville, and Y. Peings (2013), European temperatures in CMIP5: Origins of present-day biases and future uncertainties, *Clim. Dyn.*, *41*(11–12), 2889–2907, doi:10.1007/s00382-013-1731-y.
Chadee, X. T., and R. M. Clarke (2015), Daily near-surface large-scale atmospheric circulation patterns over the wider Caribbean, *Clim. Dyn.*, *44*(11–12), 2927–2946, doi:10.1007/s00382-015-2621-2.
Champion, A. J., R. P. Allan, and D. A. Lavers (2015), Atmospheric rivers do not explain UK summer extreme rainfall, *J. Geophys. Res. Atmos.*, *120*, 6731–6741, doi:10.1002/2014JD022863.
Christensen, J. H., E. Kjellstrom, F. Giorgi, G. Lenderink, and M. Rummukainen (2010), Weight assignment in regional climate models, *Clim. Res.*, *44*(2–3), 179–194, doi:10.3354/cr00916.
Cohen, J., et al. (2014), Recent Arctic amplification and extreme mid-latitude weather, *Nat. Geosci.*, *7*(9), 627–637, doi:10.1038/ngeo2234.
Corte-Real, J., B. D. Qian, and H. Xu (1998), Regional climate change in Portugal: Precipitation variability associated with large-scale atmospheric circulation, *Int. J. Climatol.*, *18*(6), 619–635, doi:10.1002/(Sici)1097-0088(199805)18:6<619::Aid-Joc271>3.0.Co;2-T.
Dacre, H. F., P. A. Clark, O. Martinez-Alvarado, M. A. Stringer, and D. A. Lavers (2014), How do atmospheric rivers form?, *Bull. Am. Meteorol. Soc.*, *96*(8), 1243–1255, doi:10.1175/BAMS-D-14-00031.1.
Davini, P., C. Cagnazzo, and J. A. Anstey (2014a), A blocking view of the stratosphere-troposphere coupling, *J. Geophys. Res. Atmos.*, *119*, 11,100–11,115, doi:10.1002/2014JD021703.
Davini, P., C. Cagnazzo, P. G. Fogli, E. Manzini, S. Gualdi, and A. Navarra (2014b), European blocking and Atlantic jet stream variability in the NCEP/NCAR reanalysis and the CMCC-CMS climate model, *Clim. Dyn.*, *43*(1–2), 71–85, doi:10.1007/s00382-013-1873-y.
Dee, D. P., et al. (2011), The ERA-Interim reanalysis: Configuration and performance of the data assimilation system, *Q. J. R. Meteorol. Soc.*, *137*(656), 553–597, doi:10.1002/Qj.828.
Demuzere, M., M. Werner, N. P. M. van Lipzig, and E. Roeckner (2009), An analysis of present and future ECHAM5 pressure fields using a classification of circulation patterns, *Int. J. Climatol.*, *29*(12), 1796–1810, doi:10.1002/Joc.1821.
Donat, M. G., G. C. Leckebusch, J. G. Pinto, and U. Ulbrich (2010), Examination of wind storms over Central Europe with respect to circulation weather types and NAO phases, *Int. J. Climatol.*, *30*(9), 1289–1300, doi:10.1002/joc.1982.
Fernandez-Montes, S., S. Seubert, F. S. Rodrigo, and E. Hertig (2012), Wintertime circulation types over the Iberian Peninsula: Long-term variability and relationships with weather extremes, *Clim. Res.*, *53*(3), 205–227, doi:10.3354/cr01095.
Fuentes, U., and D. Heimann (2000), An improved statistical-dynamical downscaling scheme and its application to the Alpine precipitation climatology, *Theor. Appl. Climatol.*, *65*(3–4), 119–135, doi:10.1007/s007040070038.
Garcia-Valero, J. A., J. P. Montavez, S. Jerez, J. J. Gomez-Navarro, R. Lorente-Plazas, and P. Jimenez-Guerrero (2012), A seasonal study of the atmospheric dynamics over the Iberian Peninsula based on circulation types, *Theor. Appl. Climatol.*, *110*(1–2), 291–310, doi:10.1007/s00704-012-0623-0.
Gleckler, P. J., K. E. Taylor, and C. Doutriaux (2008), Performance metrics for climate models, *J. Geophys. Res.*, *113*, D06104, doi:10.1029/2007JD008972.
Greve, P., and S. I. Seneviratne (2015), Assessment of future changes in water availability and aridity, *Geophys. Res. Lett.*, *42*, 5493–5499, doi:10.1002/2015GL064127.
Harnik, N., E. Galanti, O. Martius, and O. Adam (2014), The anomalous merging of the African and North Atlantic jet streams during the northern hemisphere winter of 2010, *J. Clim.*, *27*(19), 7319–7334, doi:10.1175/Jcli-D-13-00531.1.
Haylock, M. R., N. Hofstra, A. M. G. Klein Tank, E. J. Klok, P. D. Jones, and M. New (2008), A European daily high-resolution gridded data set of surface temperature and precipitation for 1950–2006, *J. Geophys. Res.*, *113*, D20119, doi:10.1029/2008JD010201.
Hoy, A., A. Schucknecht, M. Sepp, and J. Matschullat (2014), Large-scale synoptic types and their impact on European precipitation, *Theor. Appl. Climatol.*, *116*(1–2), 19–35, doi:10.1007/s00704-013-0897-x.
Huntingford, C., et al. (2014), Potential influences on the United Kingdom's floods of winter 2013/14, *Nat. Clim. Change*, *4*(9), 769–777, doi:10.1038/nclimate2314.
Hurrell, J. W. (1995), Decadal trends in the North-Atlantic Oscillation—Regional temperatures and precipitation, *Science*, *269*(5224), 676–679, doi:10.1126/science.269.5224.676.
Hurrell, J. W., and H. VanLoon (1997), Decadal variations in climate associated with the north Atlantic oscillation, *Clim. Change*, *36*(3–4), 301–326, doi:10.1023/A:1005314315270.
Huth, R. (2010), Synoptic-climatological applicability of circulation classifications from the COST733 collection: First results, *Phys. Chem. Earth*, *35*(9–12), 388–394, doi:10.1016/j.pce.2009.11.013.
Huth, R., C. Beck, A. Philipp, M. Demuzere, Z. Ustrnul, M. Cahynova, J. Kysely, and O. E. Tveito (2008), Classifications of atmospheric circulation patterns recent advances and applications, *Ann. N. Y. Acad. Sci.*, *1146*, 105–152, doi:10.1196/annals.1446.019.
Intergovernmental Panel on Climate Change (IPCC) (2013), *Climate Change 2013: The Physical Science Basis. Summary for Policymakers. Working Group I Contribution to the IPCC Fifth Assessment Report*, Cambridge Univ. Press, Cambridge, U. K.
Jones, P. D., and D. H. Lister (2009), The influence of the circulation on surface temperature and precipitation patterns over Europe, *Clim. Past*, *5*(2), 259–267.
Kidston, J., A. A. Scaife, S. C. Hardiman, D. M. Mitchell, N. Butchart, M. P. Baldwin, and L. J. Gray (2015), Stratospheric influence on tropospheric jet streams, storm tracks and surface weather, *Nat. Geosci.*, *8*(6), 433–440, doi:10.1038/ngeo2424.
Knippertz, P., and H. Wernli (2010), A Lagrangian climatology of tropical moisture exports to the northern hemispheric extratropics, *J. Clim.*, *23*(4), 987–1003, doi:10.1175/2009JCLI3333.1.
Lamb, H. H. (1972), *British Isles Weather Types and a Register of Daily Sequence of Circulation Patterns, 1861–1971*, *Geophys. Mem. 110*, 85 pp., Meteorol. Off., London.
Ludwig, P., J. G. Pinto, M. Reyers, and S. L. Gray (2014), The role of anomalous SST and surface fluxes over the southeastern North Atlantic in the explosive development of windstorm Xynthia, *Q. J. R. Meteorol. Soc.*, *140*(682), 1729–1741, doi:10.1002/qj.2253.
Madsen, H., D. Lawrence, M. Lang, M. Martinkova, and T. R. Kjeldsen (2014), Review of trend analysis and climate change projections of extreme precipitation and floods in Europe, *J. Hydrol.*, *519*, 3634–3650, doi:10.1016/j.jhydrol.2014.11.003.
Masato, G., B. J. Hoskins, and T. J. Woollings (2012), Wave-breaking characteristics of midlatitude blocking, *Q. J. R. Meteorol. Soc.*, *138*(666), 1285–1296, doi:10.1002/qj.990.
Nikulin, G., E. Kjellstrom, U. Hansson, G. Strandberg, and A. Ullerstig (2011), Evaluation and future projections of temperature, precipitation and wind extremes over Europe in an ensemble of regional climate simulations, *Tellus, Ser. A*, *63*(1), 41–55, doi:10.1111/j.1600-0870.2010.00466.x.
Pastor, M. A., and M. J. Casado (2012), Use of circulation types classifications to evaluate AR4 climate models over the Euro-Atlantic region, *Clim. Dyn.*, *39*(7–8), 2059–2077, doi:10.1007/s00382-012-1449-2.
Pattison, I., and S. N. Lane (2012), The relationship between Lamb weather types and long-term changes in flood frequency, River Eden, UK, *Int. J. Climatol.*, *32*(13), 1971–1989, doi:10.1002/joc.2415.
Perez, J., M. Menendez, F. J. Mendez, and I. J. Losada (2014), Evaluating the performance of CMIP3 and CMIP5 global climate models over the north-east Atlantic region, *Clim. Dyn.*, *43*(9–10), 2663–2680, doi:10.1007/s00382-014-2078-8.

Pfahl, S. (2014), Characterising the relationship between weather extremes in Europe and synoptic circulation features, *Nat. Hazards Earth Syst. Sci.*, *14*(6), 1461–1475, doi:10.5194/nhess-14-1461-2014.
Pfahl, S., and H. Wernli (2012), Quantifying the relevance of cyclones for precipitation extremes, *J. Clim.*, *25*(19), 6770–6780, doi:10.1175/JCLI-D-11-00705.1.
Philipp, A., et al. (2010), Cost733cat—A database of weather and circulation type classifications, *Phys. Chem. Earth*, *35*(9–12), 360–373, doi:10.1016/j.pce.2009.12.010.
Photiadou, C., B. van den Hurk, A. van Delden, and A. Weerts (2015), Incorporating circulation statistics in bias correction of GCM ensembles: Hydrological application for the Rhine basin, *Clim. Dyn.*, 1–17, doi:10.1007/s00382-015-2578-1.
Pinto, J. G., I. Gomara, G. Masato, H. F. Dacre, T. Woollings, and R. Caballero (2014), Large-scale dynamics associated with clustering of extratropical cyclones affecting Western Europe, *J. Geophys. Res. Atmos.*, *119*, 13,704–13,719, doi:10.1002/2014JD022305.
Planchon, O., H. Quenol, N. Dupont, and S. Corgne (2009), Application of the Hess-Brezowsky classification to the identification of weather patterns causing heavy winter rainfall in Brittany (France), *Nat. Hazards Earth Syst. Sci.*, *9*(4), 1161–1173.
Qian, B., J. Corte-Real, and H. Xu (2000), Nonseasonal variability of monthly mean sea level pressure and precipitation variability over Europe, *Phys. Chem. Earth Part B*, *25*(2), 177–181, doi:10.1016/S1464-1909(99)00138-0.
Ramos, A. M., N. Cortesi, and R. M. Trigo (2014a), Circulation weather types and spatial variability of daily precipitation in the Iberian Peninsula, *Front. Earth Sci.*, *2*, 25, doi:10.3389/feart.2014.00025.
Ramos, A. M., R. M. Trigo, and M. L. R. Liberato (2014b), A ranking of high-resolution daily precipitation extreme events for the Iberian Peninsula, *Atmos. Sci. Lett.*, *15*(4), 328–334, doi:10.1002/asl2.507.
Ramos, A. M., R. M. Trigo, M. L. R. Liberato, and R. Tomé (2015), Daily precipitation extreme events in the Iberian Peninsula and its association with atmospheric rivers, *J. Hydrometeorol.*, *16*(2), 579–597, doi:10.1175/JHM-D-14-0103.1.
Riahi, K., S. Rao, V. Krey, C. H. Cho, V. Chirkov, G. Fischer, G. Kindermann, N. Nakicenovic, and P. Rafaj (2011), RCP 8.5—A scenario of comparatively high greenhouse gas emissions, *Clim. Change*, *109*(1–2), 33–57, doi:10.1007/s10584-011-0149-y.
Santos, J. A., J. Corte-Real, and S. M. Leite (2005), Weather regimes and their connection to the winter rainfall in Portugal, *Int. J. Climatol.*, *25*(1), 33–50, doi:10.1002/joc.1101.
Santos, J. A., J. Corte-Real, U. Ulbrich, and J. Palutikof (2007a), European winter precipitation extremes and large-scale circulation: A coupled model and its scenarios, *Theor. Appl. Climatol.*, *87*(1–4), 85–102, doi:10.1007/s00704-005-0224-2.
Santos, J. A., J. Corte-Real, U. Ulbrich, and J. Palutikof (2007b), European winter precipitation extremes and large-scale circulation: A coupled model and its scenarios, *Theor. Appl. Climatol.*, *87*(1–4), 85–102, doi:10.1007/s00704-005-0224-2.
Santos, J. A., C. Andrade, J. Corte-Real, and S. Leite (2009a), The role of large-scale eddies in the occurrence of winter precipitation deficits in Portugal, *Int. J. Climatol.*, *29*(10), 1493–1507, doi:10.1002/joc.1818.
Santos, J. A., J. G. Pinto, and U. Ulbrich (2009b), On the development of strong ridge episodes over the eastern North Atlantic, *Geophys. Res. Lett.*, *36*, L17804, doi:10.1029/2009GL039086.
Santos, J. A., T. Woollings, and J. G. Pinto (2013), Are the winters 2010 and 2012 archetypes exhibiting extreme opposite behavior of the North Atlantic jet stream?, *Mon. Weather Rev.*, *141*(10), 3626–3640, doi:10.1175/mwr-d-13-00024.1.
Schneider, U., A. Becker, P. Finger, A. Meyer-Christoffer, M. Ziese, and B. Rudolf (2014), GPCC's new land surface precipitation climatology based on quality-controlled in situ data and its role in quantifying the global water cycle, *Theor. Appl. Climatol.*, *115*(1–2), 15–40, doi:10.1007/s00704-013-0860-x.
Screen, J. A. (2013), Influence of Arctic sea ice on European summer precipitation, *Environ. Res. Lett.*, *8*(4), 044015, doi:10.1088/1748-9326/8/4/044015.
Seneviratne, S. I., et al. (2012), Changes in climate extremes and their impacts on the natural physical environment, in *Managing the Risks of Extreme Events and Disasters to Advance Climate Change Adaptation*, edited by C. B. Field et al., pp. 109–230, Cambridge Univ. Press, Cambridge, U. K.
Sillmann, J., V. V. Kharin, X. Zhang, F. W. Zwiers, and D. Bronaugh (2013a), Climate extremes indices in the CMIP5 multimodel ensemble: Part 1. Model evaluation in the present climate, *J. Geophys. Res. Atmos.*, *118*, 1716–1733, doi:10.1002/jgrd.50203.
Sillmann, J., V. V. Kharin, F. W. Zwiers, X. Zhang, and D. Bronaugh (2013b), Climate extremes indices in the CMIP5 multimodel ensemble: Part 2. Future climate projections, *J. Geophys. Res. Atmos.*, *118*, 2473–2493, doi:10.1002/jgrd.50188.
Small, R. J., R. A. Tomas, and F. O. Bryan (2014), Storm track response to ocean fronts in a global high-resolution climate model, *Clim. Dyn.*, *43*(3–4), 805–828, doi:10.1007/s00382-013-1980-9.
Sousa, J. F., M. Fragoso, S. Mendes, J. Corte-Real, and J. A. Santos (2013), Statistical–dynamical modeling of the cloud-to-ground lightning activity in Portugal, *Atmos. Res.*, *132–133*, 46–64, doi:10.1016/j.atmosres.2013.04.010.
Taylor, K. E., R. J. Stouffer, and G. A. Meehl (2012), An overview of CMIP5 and the experiment design, *Bull. Am. Meteorol. Soc.*, *93*(4), 485–498, doi:10.1175/Bams-D-11-00094.1.
Trigo, R. M., and C. C. DaCamara (2000), Circulation weather types and their influence on the precipitation regime in Portugal, *Int. J. Climatol.*, *20*(13), 1559–1581, doi:10.1002/1097-0088(20001115)20:13<1559::Aid-Joc555>3.0.Co;2-5.
Tveito, O. E. (2010), An assessment of circulation type classifications for precipitation distribution in Norway, *Phys. Chem. Earth*, *35*(9–12), 395–402, doi:10.1016/j.pce.2010.03.044.
Ulbrich, U., M. Christoph, J. G. Pinto, and J. Corte-Real (1999), Dependence of winter precipitation over Portugal on NAO and baroclinic wave activity, *Int. J. Climatol.*, *19*(4), 379–390, doi:10.1002/(sici)1097-0088(19990330)19:4<379::aid-joc357>3.0.co;2-8.
van Vuuren, D. P., et al. (2011), The representative concentration pathways: An overview, *Clim. Change*, *109*(1–2), 5–31, doi:10.1007/s10584-011-0148-z.
Wernli, H., S. Dirren, M. A. Liniger, and M. Zillig (2002), Dynamical aspects of the life cycle of the winter storm 'Lothar' (24–26 December 1999), *Q. J. R. Meteorol. Soc.*, *128*(580), 405–429, doi:10.1256/003590002321042036.
Wilks, D. S. (2011), *Statistical Methods in the Atmospheric Sciences*, 2nd ed., xvii, 627 pp., Academic, Boston, Mass.
Woollings, T., A. Hannachi, and B. Hoskins (2010), Variability of the North Atlantic eddy-driven jet stream, *Q. J. R. Meteorol. Soc.*, *136*(649), 856–868, doi:10.1002/qj.625.
Woollings, T., J. G. Pinto, and J. A. Santos (2011), Dynamical evolution of North Atlantic ridges and poleward jet stream displacements, *J. Atmos. Sci.*, *68*(5), 954–963, doi:10.1175/2011jas3661.1.
Woollings, T., C. Czuchnicki, and C. Franzke (2014), Twentieth century North Atlantic jet variability, *Q. J. R. Meteorol. Soc.*, *140*(680), 783–791, doi:10.1002/qj.2197.
Zappa, G., M. Hawcroft, L. Shaffrey, E. Black, and D. Brayshaw (2014), Extratropical cyclones and the projected decline of winter Mediterranean precipitation in the CMIP5 models, *Clim. Dyn.*, *45*, 1727–1738, doi:10.1007/s00382-014-2426-8.
Zappa, G., B. J. Hoskins, and T. G. Shepherd (2015), Improving climate change detection through optimal seasonal averaging: The case of the North Atlantic jet and European precipitation, *J. Clim.*, doi:10.1175/JCLI-D-14-00823.1, in press.